THE HIGH-FREQUENCY CHARACTERISTICS OF SOLAR RADIO BURSTS

J. LIM, S. M. WHITE, M. R. KUNDU

Department of Astronomy, University of Maryland, College Park, MD 20742, U.S.A.

and

D. E. GARY

Solar Astronomy 264–33, Caltech, Pasadena, CA 9110, U.S.A.

(Received 6 February, 1992; in revised form 6 March, 1992)

Abstract. We compare the millimeter, microwave, and soft X-ray emission from a number of solar flares in order to determine the properties of the high-frequency radio emission of flares. The millimeter observations use a sensitive interferometer at 86 GHz which offers much better sensitivity and spatial resolution than most previous high-frequency observations. We find a number of important results for these flares: (i) the 86 GHz emission onset appears often to be delayed with respect to the microwave onset; (ii) even in large flares the millimeter-wavelength emission can arise in sources of only a few arc sec dimension; (iii) the millimeter emission in the impulsive phase does not correlate with the soft X-ray emission, and thus is unlikely to contain any significant thermal bremsstrahlung component; and (iv) the electron energy distributions implied by the millimeter observations are much flatter (spectral indices of 2.5 to 3.6) than is usual for microwave or hard X-ray observations.

1. Introduction

The properties of radio emission from solar flares at millimeter wavelengths are poorly known. The reasons for this are well understood: the telescopes available have generally had poor sensitivity and poor spatial resolution compared with those available at microwave wavelengths in the last 20 years. However, there is much that can be learnt from millimeter observations which the microwave observations do not provide. In particular, millimeter observations of solar flares are sensitive to the most energetic electrons, and they are almost always optically thin so that one sees all the electrons present radiating, unlike observations which are usually dominated by the optically-thick component.

It has long been known that the high-frequency spectrum of radio emission can be used to study the energy distribution in flares, but because of the lack of sensitive high-frequency observations the high-frequency spectral indices are generally only known for a small number of very large flares. Croom and Powell (1969) observed a giant flare with a spectrum still rising at 71 GHz (peak flux 47000 s.f.u.); Croom (1970) reported 71 GHz observations including one flare with a complex spectrum but apparently falling off sharply at 71 GHz, and another with a spectrum flat beyond 35 GHz; Shimabukuro (1970, 1972) reported a number of flares with spectra flat at high frequencies, and he and Hudson and Ohki (1972) demonstrated that these spectra could be associated with the thermal soft-X-ray emitting material seen in the decay phase of

Solar Physics **140:** 343–368, 1992.

flares. Hachenberg and Wallis (1961) had originally suggested a thermal bremsstrahlung interpretation for spectra observed to be flat up to 30 GHz. Akabane *et al.* (1973) also demonstrated that the millimeter component did not correlate well with the microwave gyrosynchroton component. Kaufmann *et al.* (1986) have compiled the high-frequency spectra of a small number of bursts from the above references on one figure.

However, all of these observations were made with single-dish millimeter telescopes, which were limited in sensitivity in both the state of millimeter receivers at the time, and by atmospheric effects which are strong at short wavelengths. Thus all the flares were very large, and cannot be considered 'typical' of solar flares. Evidence of this may be seen in the fact that Croom (1970) observed only seven flares in over 2 years of nearly continuous monitoring at a solar maximum. Large flares are notoriously complicated and accordingly difficult to analyze.

Millimeter interferometers offer much better sensitivity and spatial resolution than do single-dish telescopes, since they are not sensitive to the large solar thermal flux and are less sensitive to atmospheric effects. The first interferometric measurement of solar mm-wave flares was reported by Kawabata *et al.* (1982). These observations were made at the relatively long wavelength of 8 mm (i.e., 35 GHz) with the Nagoya fan-beam interferometer. Several very strong flares were detected; all of those flares with peak flux densities above 300 s.f.u. were accompanied by γ-ray flares. Because γ-rays are believed to be producted by relativistic electrons precipitating into the dense transition region and chromosphere, Kawabata *et al.* (1982) suggested that the radio emission also was produced by relativistic electrons radiating through the gyrosynchroton process.

Much more sensitive observations at shorter wavelengths (3 mm) have now become possible with the development of large multi-element interferometric arrays. Kundu *et al.* (1990) used the Berkeley–Illinois–Maryland Array (BIMA) to study flares during the high activity of 1989 March. With an unprecedented sensitivity of about 0.03 s.f.u., they found that virtually every flare within the telescope field-of-view was detected, and that the high-frequency spectra were generally falling. However, the time resolution of these observations ($\sim$20 s) was not adequate for a detailed study of the spectra.

Theoretical computations by Ramaty (1969), Holt and Ramaty (1969), and Ramaty and Petrosian (1972) show that gyrosynchrotron emission at mm-wavelengths in the corona requires electrons with relativistic energies (i.e., $E \gtrsim 1$ MeV). Thus, if electrons are accelerated to relativistic energies during the impulsive phase they are expected to be accompanied by impulsive millimeter emission. Because the emission at millimeter wavelengths is optically thin, the spectral index of the radiation is a direct measure of the energy spectrum of the radiating electrons; furthermore, the intensity of the flare at mm-wavelengths can be used to estimate the total kinetic energy of the electrons.

Some observations of flares in the millimeter range have shown results quite different from that expected on the basis of gyrosynchroton models for radio emission deduced from microwave observations. Kaufmann *et al.* (1985) report a flare which displayed quasi-periodic oscillations at mm-wave, no detectable microwave emission, and a spectrum rising from 30 to 90 GHz (peak flux of 70 s.f.u. at 90 GHz; observed with the large single-dish telescope at Itapetinga). By contrast, the small burst reported by White

et al. (1992) displayed a fast rise followed by a slow decay, and flat spectrum from 15 to 86 GHz. The properties of these flares are difficult to reconcile with gyrosynchrotron emission from energetic electrons (White *et al.*, 1992), and indeed are unexpected if impulsive mm-wave flares are simply extensions to higher electron-energies of their counterparts at microwave. Instead the remarkable properties of these flares suggest that they may have been exceptional events. Clearly a systematic study of impulsive mm-wave flares is required to establish their gross properties, and to distinguish between the commonly occurring events and the truly exceptional.

In this paper we present a systematic study of solar flares at millimeter wavelengths with high sensitivity, and high temporal and spatial resolution. A detailed comparison of the high frequency radio emission with microwave soft-X-ray behaviour is carried out. By using the technique of interferometry, we largely resolve out the bright quiet-Sun-background and intense thermal emission from extended sources and this allows us to study the impulsive phase of even small flares at millimeter wavelengths. A comparison of the millimeter and microwave behaviour reveals a close temporal relationship between their impulsive phases, suggesting therefore that indeed mm wavelength emission in the impulsive phase is produced by the gyrosynchrotron mechanism. With the combination of high sensitivity and time resolution we have found a distinct time delay between the onset of a few flares at microwave and mm wavelengths, with the emission beginning first at lower frequencies.

We describe the observations in the next section, and the analysis of the data in the following section. The main part of the paper (Section 4) is a comparison of millimeter, microwave and soft X-ray behaviour of 6 flares ranging in soft X-ray size from C4.9 to X2; because of the lack of such detailed comparisons in the literature we discuss each flare in some detail. We discuss the results in Section 5; however, detailed interpretation of these observations in terms of flare models will be deferred to a later paper in which comparisons of millimeter and hard X-ray observations are available.

2. Observations

We used the Berkeley–Illinois–Maryland Array (BIMA) to monitor the solar active region AR 6538 from approximately 15:35 to 00:45 UT daily on 1991 March 6–8. The array presently comprises three movable 6-m parabolic antennas located at stations arranged in a 'T' configuration. These antennas accept signals in two 40-MHz sidebands centered at frequencies of 86.24 and 89.44 GHz (i.e., wavelenghts of about 3.5 mm) respectively. For each pair of antennas, the signals in each of the two-sidebands are correlated to produce a one-dimensional spatial Fourier transform of the sky brightness distribution (i.e., visibilities consisting of an amplitude and phase for each baseline) within the primary beam of the telescope. The measured phase on each baseline, when correctly calibrated, is a measure of the position of the centroid of the brightness distribution with respect to the pointing center of the telescope in units of the fringe spacing.

For observations of solar flares, BIMA is presently used as an interferometer in one linear polarization (equivalent to Stokes I) with 3 baselines (see White *et al.*, 1992). At the time of these observations the array was in a wide configuration, corresponding to high spatial resolution at the expense of information on large spatial scales. With the antennas at 134.1 m west, 24.4 m east, and 97.5 m north of array center, the fringe spacings of the interferometer on the sky when the Sun crossed the meridian were 4.5″, 9.8″, and 4.8″ on baselines 12, 23, and 31, respectively. An interferometer is insensitive to sources much larger than about one-third of the fringe spacing. AR 6538 covered a large area, and since the field-of-view of BIMA is restricted (2′), on each day the telescope was pointed at the site of greatest flaring activity on the previous day, as judged from the number of Hα flares. The time resolution of the measurements was 0.39 s, with an integration time of 0.32 s. The array was calibrated in amplitude using observations of 3C454 interspersed through the solar observations.

In order to study the radio spectra of the flares observed by BIMA we have analyzed the microwave observations for this period from the frequency-agile interferometer at the Owens Valley Radio Observatory (OVRO), and also from the RSTN network of patrol telescopes. The OVRO microwave array presently comprises two 7-m and three 2-m antennas situated on a T-shaped railtrack (see overview by Hurford, Read, and Zirin, 1984). On March 6 to 8 only the two 27-m antennas were in regular operation, with two of the three 2-m antennas being used only for a short period on March 7. The two 27-m antennas were separated by 426.7 m along an east–west direction. Linked as an interferometer they measured the brightness distribution of the sky at 45 separate frequencies, spaced at nearly regular logarithmic intervals from 1.0 to 18.0 GHz, in left and right circular polarization consecutively. The time taken to cycle through all 45 frequencies in each circular polarization was 10.0 s. The single-dish total power at each of the 45 frequencies in left-circular, right-circular, and linear polarization also was measured every 10.2 s. The array was calibrated in amplitude and phase by observing a strong compact source at approximately 2-hour intervals. During March 6 to 8 the telescope was pointed at the nominal position of the active region AR 6538, which was away from the site of greatest flaring activity. Although this was not a serious problem at frequencies below about 10 GHz where the half-power beamwidth of the telescope is large ($\gtrsim$4 arc min), at higher frequencies flares originating from the site observed by BIMA were occasionally only barely detectable by OVRO.

Data from the RSTN patrol telescope network were provided by the facilities at Sagamore Hill and Palehua. These telescopes observe the entire solar disk at frequencies of 0.24, 0.41, 0.61, 1.4, 2.7, 5.0, 8.8, and 15.4 GHz simultaneously. We will not discuss the lower-frequency observations.

To investigate the contribution of flare-heated high-temperature ($T > 10^7$ K) plasma to the radio emission, we also obtained the soft X-ray data obtained by the GOES satellite (courtesy of G. Labow, NASA/GSFC). This telescope observes the entire solar disk in two energy channels, spanning the energy ranges 1.5 to 10 keV and 3 to 25 keV.

3. Data Reduction and Analysis

The visibilities measured by BIMA were calibrated in Stokes I for each of the three interferometer baselines in each side-band. At present the accuracy of the amplitude calibration is believed to be $\sim 30\%$. The three antennas were also calibrated in total power, although only very strong flares could be detected in total power. The data were then inspected for fluctuations in amplitude due to radio bursts. For these bursts the unresolved quiet-Sun emission was removed by calculating an average of the visibilities measured immediately prior to the burst and subtracting this average from the data.

Since three antennas are insufficient to map burst sources on short time-scales we use the concept of closure phase to estimate source dimension and structure from BIMA data (White and Kundu, 1992). The closure phase is the sum of the phases measured on each of the three baselines. It is independent of antenna-based errors such as atmospheric effects. A constant closure phase in the BIMA data indicates that the source is unresolved, or that its brightness temperature distribution is axially symmetric about a distinct peak (the constant phase value will not in general be zero due to known errors in the analog correlator, but the value does not vary much on a time scale of hours). A non-constant closure phase indicates that the source may be much larger than the available fringe spacings can 'see', highly asymmetric, or evolving with time.

At the OVRO microwave array, absolute phase calibration is done by using monthly calibrations on 3C84, with daily corrections made by observing secondary calibrators about every 2 hours. The phase of the daily calibrator observations are calibrated against the 3C84 reference phase, leaving residual phases that deviate from zero only linearly with frequency. These residual phases can change during the day, due to changing ambient conditions, but can be fit with a single straight line to yield a frequency-dependent correction that is then applied to the solar data. The visibility amplitude is calibrated with respect to 3C84, which is in turn calibrated with respect to 3C286. The total power is calibrated by comparison with the power flux of Cas A.

Data from the OVRO array were inspected visually for microwave bursts which occurred closely in time to those observed at BIMA. For these flares the unresolved quiet Sun emission was removed from the measured visibilites, and total power, using the same subtraction procedure as for the BIMA data.

Data from Sagamore Hill and Palehua were already calibrated in intensity. They were inspected visually for microwave bursts which occurred closely in time to the observed mm-wave bursts. For these bursts the contribution from the quiet Sun was removed by subtracting the flux density measured immediately prior to the flare from that measured during the flare.

We describe in the following only bursts with good signal-to-noise ratios at both microwave and mm wavelengths. A few flares which met these criteria were excluded, however, because of large gaps in the mm-wave data caused by bad antenna pointing (which occurred during periods of strong wind).

4. Results

A total of thirteen mm-wave bursts (with peak correlated amplitudes ranging from 0.2 to 1.50 s.f.u.) were detected by BIMA during these observations: five each on March 6 and 7, and the remaining three on March 8. Of these four were excluded from further analysis because of bad antenna pointing in high wind, and two because of their poor signal-to-noise ratios. Furthermore, one other mm-wave flare was excluded because of its surprisingly weak microwave emission; this event will be discussed elsewhere. The remaining six mm-wave bursts (three each on March 7 and March 8) were all accompanied by microwave bursts, and their properties are described in detail below.

The OVRO microwave array can potentially provide accurate spectra and fluxes of flares over the entire frequency range from 1 to 18 GHz, provided that is the flare is within the nominal field of view of the telescope. Unfortunately, because of the size of AR 6538 the centroids of most of the flares reported here were about 1 arc min or more from the phase tracking centre of the telescope. The half-width half-power point of the OVRO 27 m dishes at a frequency f GHz is $19'/f$. As a consequence, at high frequencies the actual flux of the flare was not well determined, and could not be accurately derived from the observations because of the poorly determined side-lobe response of the telescope. Thus we will use the RSTN data for information on the spectra of the bursts, and also for the flux at high frequencies (i.e., 15 GHz). The OVRO data nevertheless provided information about the polarization and spatial structure of the flare (in one-dimension) which could not be obtained from the RSTN data. The fringe spacing of the OVRO observations is $2.4'/f$.

In the remainder of this section we will discuss the properties of the six flares (from 3C, to 2X GOES class) in some detail because the properties of flares, particularly small flares, at millimeter wavelengths are poorly known.

4.1. Flare 1

This optical-class SF flare on March 7 has a start time of 18:39 UT reported in *Solar-Geophysical Data*. Emission at 86 GHz began at 18:42:15 UT, and had a total duration of about 2 min. The accompanying flare was observed at Sagamore Hill, but not at OVRO because it occurred during a calibration scan. The reported optical flare location was 34″ from the center of the BIMA field-of-view; the half-power points of the BIMA primary beam are at 1.2′, so we expect only a small loss of flux due to the primary beam pattern.

The temporal profiles of this flare at 5.0, 8.8, 15.4, and 86.0 GHz are shown in Figure 1; the measured closure phase at 86.0 GHz also is shown on this figure. This flare had a short rise-time, followed by a more gradual exponential-like decay. At 86 GHz there are two peaks: one associated with the single peak at 15.4 GHz, and another occurring 20 s later which may be visible in the microwave data but is certainly relatively less prominent there. The peak flux at 8.8 GHz was sufficiently small that no microwave report was given for the event in *Solar-Geophysical Data*.

The peak flux of this burst reached 3, 13, 75, and 9 s.f.u. at 5.0, 8.8, 15.4, and

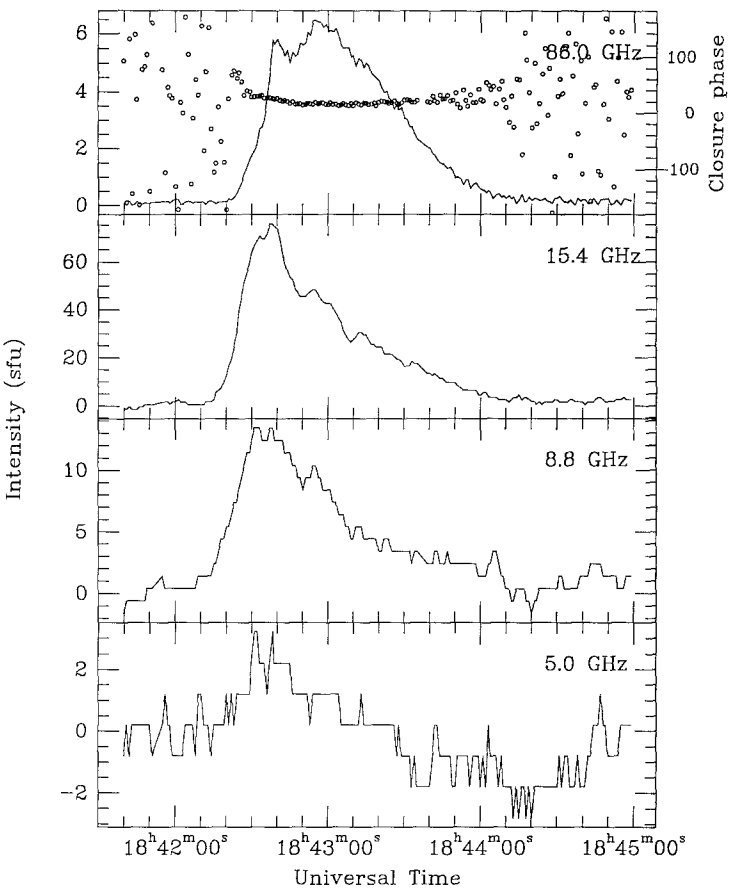

Fig. 1. Time profile of flare 1 at 5.0, 8.8, 15.4 (all RSTN total power measurements), and 86.0 GHz (BIMA correlated amplitude on baseline 12). In the top panel we also plot the closure phase on the lower sideband for the 86 GHz data (scale on the right-hand axis).

86.0 GHz, respectively. Thus the microwave flare spectrum has a positive spectral index between 5.0 and 15.4 GHz (spectral index of + 2.6 from 5.0 to 8.8 GHz and of + 3.1 from 8.8 to 15.4 GHz; the typical value for a homogeneous optically-thick gyrosynchrotron spectrum is + 2.8), and its turnover frequency appears to be above 15.4 GHz. The majority of microwaves flares have turnover frequencies between 5 and 10 GHz (Guidice and Castelli, 1975). If we assume that the turnover frequency is at 15.4 GHz, then during the rise phase of the flare the spectral index between 15.4 and 86.0 GHz is about − 1.2.

To permit a more detailed comparison, the temporal profiles of the flare at 15.4 and 86.0 GHz are plotted together in Figure 2. We plot two baselines for 86 GHz: baseline 23, with a fringe spacing of 10.4″, and baseline 12 with a fringe spacing of 4.4″. The profile on baseline 31 was essentially identical to that on 12. The soft X-ray behaviour in the energy range 3 to 25 keV is also plotted on this figure. No GOES soft X-ray class was assigned to this flare in *Solar-Geophysical Data*; the soft X-ray flux at this time was

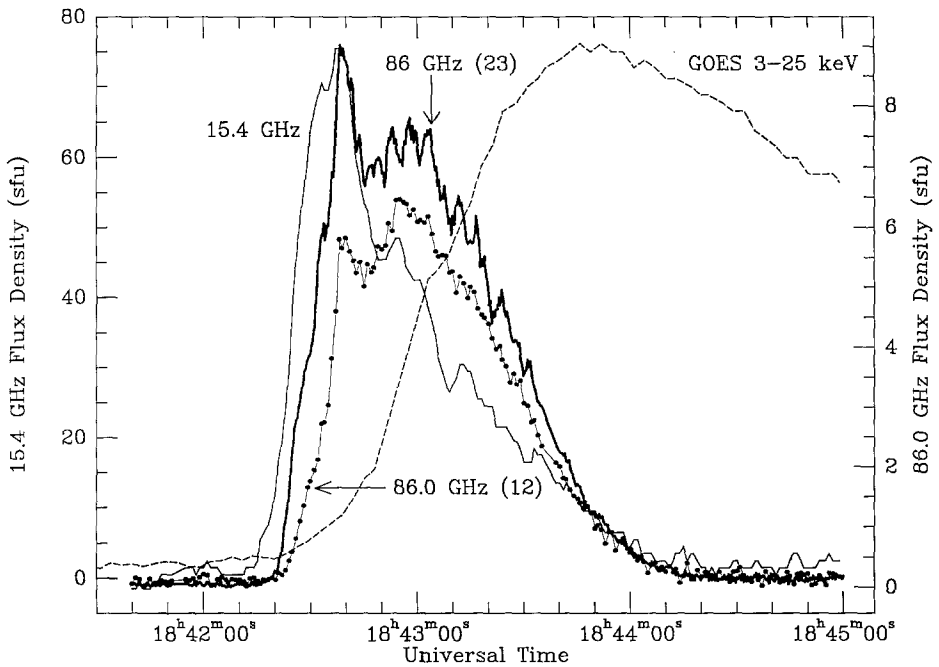

Fig. 2. Comparison of the time profile of flare 1 at 15.4 GHz (RSTN data, thin solid line; the scale is given on the left-hand axis), at 86.0 GHz on baseline 23 with fringe spacing 10″ (thick solid line; scale on right-hand axis), at 86.0 GHz on baseline 12 with fringe spacing 4″ (filled circles), and in 3–25 keV soft X-rays (broken line) as measured by the GOES satellite (plotted on a linear scale, not shown: this flare reached about GOES class C6). The time resolution is 1 s at 15.4 GHz, 0.4 s at 86 GHz, and 3 s in soft X-rays.

still above C5 level due to the slow decay of an X5.5 event 12 hours earlier, but a small enhancement to C6 level at the time of the flare is clearly visible in the GOES curve. The soft X-ray flare begins at approximately the same time or just after the onset of the radio flare. It is clear by comparison of the GOES and 86 GHz profiles that there is little or no contribution at 86 GHz from the soft-X-ray emitting thermal material, and we therefore assume that most of the 86 GHz emission is due to gyrosynchrotron emission by energetic electrons. We estimate that the contribution at 86 GHz due to the soft X-ray emitting material seen by GOES was only about 0.4 s.f.u. at the GOES peak (calculated according to the formulae of Thomas, Start, and Crannell, 1985; see White and Kundu 1992). The soft X-ray emitting material can be assumed to be optically thin at high radio frequencies, which leads to a flat flux spectrum for its contribution.

As can be seen there appears to be a time delay of ~ 5 s between the onsets at 15.4 and 86.0 GHz, with the emission beginning earlier at the lower frequency. We will show that this time delay was not a consequence of different effective detection thresholds at these two frequencies, but indicates a real frequency dependence in the onset of the flare. The spectral index between 15.4 and 86.0 GHz increases monotonically from about -2.0 to -1.2 between the onset of the flare and its peak; let us therefore assume a

spectral index of -2.0 at the beginning of the flare. The flux density of this flare five seconds after its onset at 15.4 GHz was ~ 13 s.f.u., at which time the flux density at 86.0 GHz (for a spectral index of -2.0) should have been ~ 0.4 s.f.u. By contrast, at this time the flux density at 86.0 GHz was still consistent with noise at level below 0.2 s.f.u., which is much less than that expected if the flare onset was simultaneous at the two frequencies.

Although its flux density at 86 GHz is about an order of magnitude less than that at 15.4 GHz, the overall temporal profiles of the flare in the two different bands are quite similar; the primary and secondary peaks at microwaves (centered at 18:42:35 and 18:42:55, respectively) are apparent also at 86 GHz, but comparison of the two 86 GHz curves shows that the relative sizes of the two peaks differed on the different baselines. The largest flux at 86 GHz was seen on the shortest baseline (23, i.e., the baseline with the largest fringe spacing), as expected. The closure phase at 86 GHz (Figure 1) remains constant throughout the lifetime of the flare, indicating that the flaring source has a simple structure at the scale of the fringe spacings available (approximately 4.7″, 10.4″, and 4.4″). This means that the 86 GHz emission is probably dominated by a single source of dimension no larger than a few arc sec. The observed visibility amplitude on the shortest baseline is therefore probably an accurate measure of the actual intensity of the flare.

4.2. Flare 2

This was a GOES class M1.5 flare with optical class SN. The optical start is listed as 20:39 UT (March 7); emission at 86 GHz began at approximately 20:37 UT, and had a total duration of about 13 min. The accompanying microwave flare was observed at both OVRO and Sagamore Hill. The temporal profiles of this flare at 5, 8.8, 15.4, and 86 GHz, and the closure phase at 86 GHz, are shown in Figure 3. The optical flare location was 20″ from the BIMA pointing center, and 100″ from the OVRO pointing center.

The microwave flare had a complex morphology, with a primary peak dominated by a sharp single spike just after onset at 20:38:30, followed by a much weaker secondary peak at 20:44:00. At 86 GHz the time profile of the flare showed considerable differences on the three baselines (with fringe spacings of about 5″, 9″, and 6″, respectively). In particular, the initial peak was strongest (7 s.f.u.) on baseline 31, while the subsequent peak was strongest (6 s.f.u.) and larger than the initial peak on baseline 23. It is clear from these differences that at 86 GHz BIMA was missing a substantial fraction of the total flux from this burst. The behaviour of the closure phase at 86 GHz is consistent with this: it varied throughout the lifetime of the flare. There is a brief period during the initial peak at 86 GHz where the closure phase is roughly constant, at the same value that was seen during flare 1, and at this time the 86 GHz emission may have been dominated by a simple source. The initial microwave peak was unresolved by OVRO at 8 GHz with a fringe spacing of 18″, indicating a source size (in one-dimension) of less than 5″ (the flare was outside the nominal field of view at higher frequencies). The

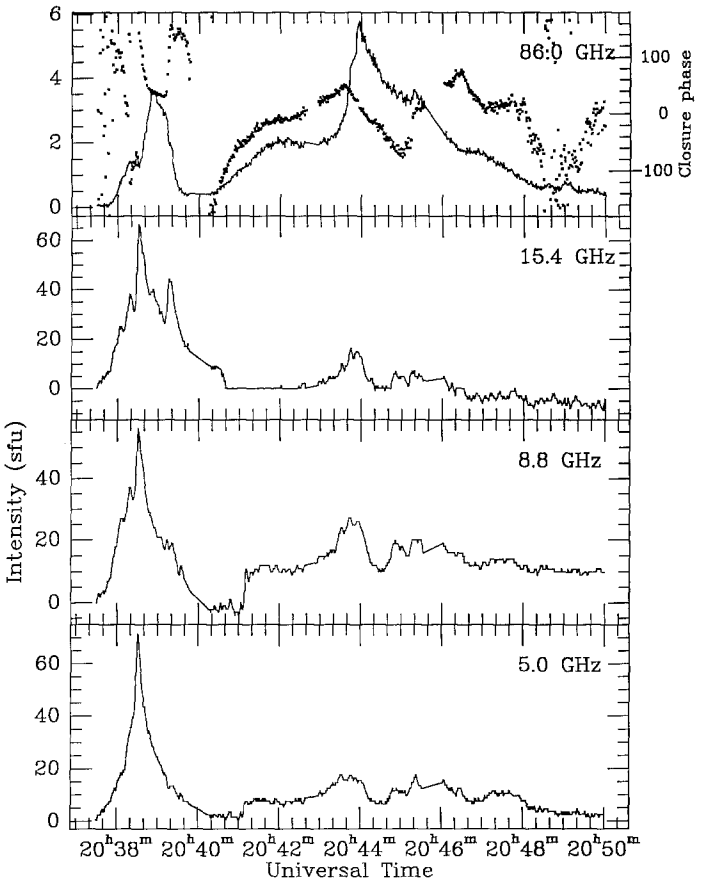

Fig. 3. Time profile of flare 2 at 5.0, 8.8, 15.4, and 86.0 GHz (baseline 23); format as in Figure 1.

measured visibility phase at microwaves was the same for both the primary and secondary peaks, indicating a common emission site.

The temporal profiles of the first peak at 15.4 and 86.0 GHz (for two different baselines at 86 GHz) are shown in Figure 4, along with the soft X-ray time profile. As with flare 1, the soft X-ray emission apparently begins after the impulsive phase in radio. There is a delay of 20 s between the 15.4 GHz peak and the 86 GHz peak on both baselines. The slow rise of the event prevents us from obtaining any evidence on the relative onset times of emission at 15.4 and 86 GHz. Note the small peak at 20:39:20, in the decline after the main peak, which shows up simultaneously at 15.4 GHz and on baseline 31 at 86 GHz.

The RSTN data show that, except for the fine structure, the spectrum between 5.0 and 15.4 GHz was essentially flat throughout the lifetime of the flare. The superior frequency coverage of OVRO indicates that the turnover frequency of the second peak may have been higher than that of the first peak. This would be consistent with the ratio of the peak flux density of the second to the first peak being higher at mm-wave than

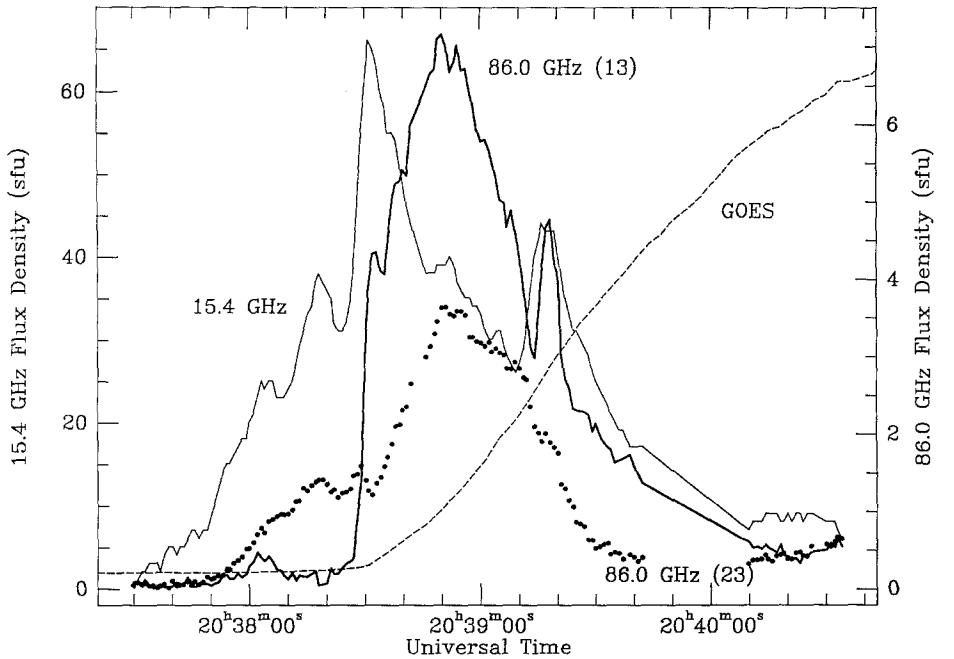

Fig. 4. Comparison of time profiles of the first two minutes of flare 2 at 15.4 GHz (thin solid line), 86.0 GHz on baselines 31 (thick solid line) and 23 (filled circles), and in 3–25 keV soft X-rays (broken line).

in microwaves. At the first microwave peak (20:28:30 UT) the spectral index between 15.4 and 86.0 GHz (for baseline 31 where the flux was greatest) was approximately − 1.6. At the first millimeter peak (20:38:50 UT) it was − 1.0; at the second millimeter peak (20:44 UT) it was about − 0.7. Note that since we are assuming that the 86 GHz data underestimate the true flux, these values of spectral index are lower limits to the real spectral index between 15.4 and 86 GHz. These rather flat spectra suggest that optically thin thermal bremsstrahlung may be playing a substantial role in the emission. However, at least in the initial peak, it is clear that the GOES profile does not match any of the radio profiles, and so any thermal material present must be a different population from the hot plasma producing the soft X-ray emission. The contribution from the GOES material at 86 GHz during the first impulsive peak is less than 1 s.f.u.; it peaks ar 4 s.f.u. at about 20:42 and declines thereafter, showing no peak corresponding to the secondary radio peak at 20:44 UT.

4.3. Flare 3

This was an optical class 1B flare with a soft X-ray class of X2.5 which began at about 23:13 on 1991 March 7. Emission at 86 GHz began at approximately 23:16:55 UT, and, remarkably for an X-class flare, the radio emission (microwave and milimeter) has a total duration of only about 3 min. The flare produced the largest correlated amplitude yet seen at BIMA. The accompanying microwave flare was observed at both Palehua

and OVRO. The temporal profile of this flare at 5, 8.8, 15.4, and 86 GHz, and its closure phase at 86 GHz, is shown in Figure 5. The microwave flare had a short rise and decay time, and two main peaks with the second peak being more intense than the first. The optical flare location was 30″ from the BIMA pointing center, and 117″ from the OVRO pointing center.

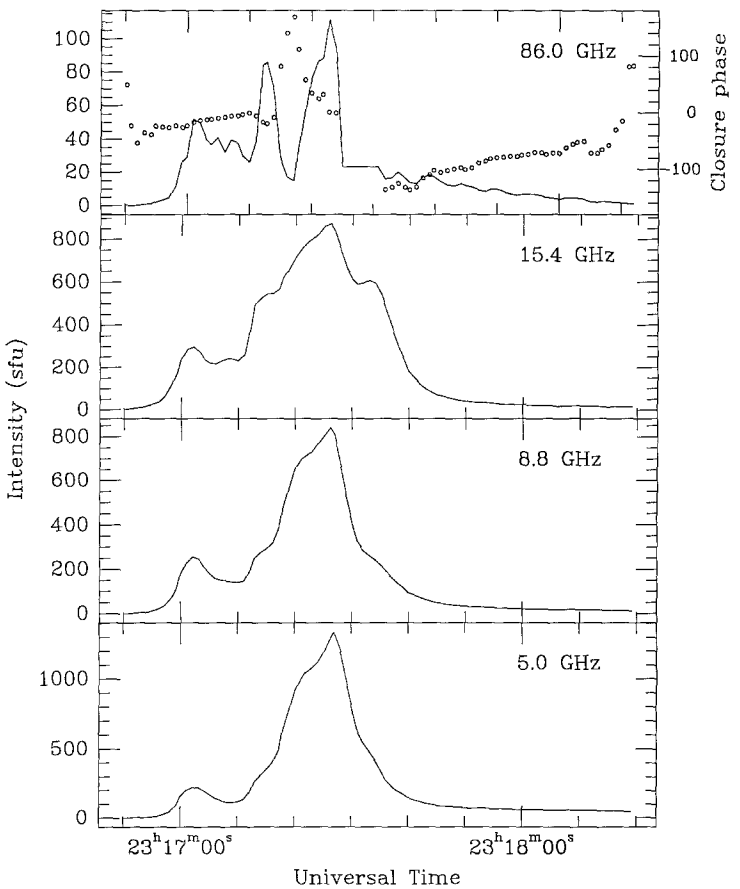

Fig. 5. Time profile of flare 3 at 5.0, 8.8, 15.4, and 86.0 GHz (baseline 23); format as in Figure 1.

The temporal profiles of the flare at 15.4 and 86.0 GHz (two baselines shown), along with the soft X-ray burst, are plotted together in Figure 6. There is no discernible time delay between the onset of the flare at 15.4 and 86 GHz, after the different effective detection thresholds at the two frequencies are taken into account. There is a data gap at 86 GHz due to bad antenna pointing in strong wind which may be seen from 23:17:27 to 23:17:40, and a low-level high-frequency oscillation in the decay phase on baseline 23 at 86 GHz which is believed to be instrumental. Like the two previous flares, the soft X-ray emission appears to begin after the impulsive phase in radio.

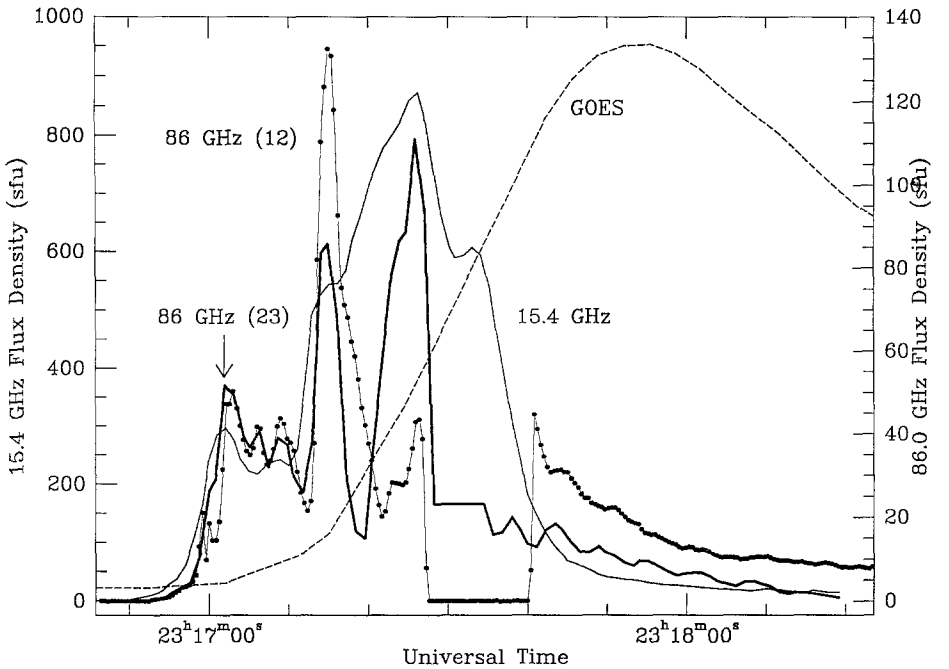

Fig. 6. Comparison of time profiles of flare 3 at 15.4 GHz (thin solid line), 86.0 GHz on baselines 23 (thick solid line) and 12 (filled circles joined by narrow solid line), and in 3–25 keV soft X-rays (broken line).

The time profiles at 86 GHz contain multiple peaks, which we attribute to the effects of the source being much larger than the available fringe spacings could 'see' (the fringe spacings were about 9″, 7″, and 12″ on baselines 12, 23, and 31, respectively). This may be understood by remembering that the correlated amplitude is the integral of the brightness distribution convolved with a sinusoidal function of the appropriate fringe spacing; as different parts of the source brighten and fade, or as the source expands, we get different contributions in the positive and negative lobes of the sinusoid. The integral goes up and down accordingly. Consistent with this interpretation is the fact that, as can be seen from Figure 6, the profiles on different 86 GHz baselines were different (baseline 31 was similar to baseline 23 in flux and profile); however, with the exception of a sharp peak at 23:17:15, the 86 GHz peaks fit well within an envelope which has the shape of the 15.4 GHz profile.

We believe that this burst had a fairly simple structure on a spatial scale of a few arc sec at least for the first 20 s. The closure phase of the flare at 86 GHz remains constant until changing abruptly during the evolution of the largest peak (Figure 5). Furthermore, the fluxes measured on all three baselines were the same to within about the accuracy of the absolute calibration at 86 GHz until the peak at 23:17:15 (Figure 6). Thus until 23:17:15 the 86 GHz source may well have been smaller than 2″; if so, the corresponding effective brightness temperature was in excess of 5×10^7 K. We assume that the peak at 23:17:15 corresponds to the presence of a very hard component in the

electron distribution, since it was seen by all 3 baselines at 86 GHz but was barely present at 15.4 GHz (see below); thereafter we believe that the size of the source was much larger so that the variations in correlated amplitude might no longer correspond well with variations in the true flux at 86 GHz. The peak of the microwave flare was well resolved by OVRO at 15 GHz with a fringe spacing of 19″, so by that stage the microwave source size must have been greater than about 6″.

The soft X-ray behaviour of this flare is remarkable for an X-class flare in the lack of an extended decay phase: both the 1.5–12.5 keV and 3–25 keV channels return almost to their preflare levels some 10 min after flare onset. The soft X-ray emission was also the hardest of the six flares discussed here, corresponding to a temperature of almost 2×10^7 K. Therefore, we speculate that this flare belongs to the class of confined flares, occurring in strong magnetic fields which do not permit much expansion of the hot dense plasma in the corona in the post-flare phase (Schmahl *et al.*, 1990).

The microwave spectrum appears to be consistent with this interpreation. The microwave observations show a spectral index of ~ 1.0 between 1.4 and 5.0 GHz, and an essentially flat or slightly decreasing spectrum between 5.0 and 15.4 GHz, exactly as in the case studied by Schmahl *et al.* (1990). This could put the turnover frequency above 15.4 GHz, as one expects for a source in a region of high magnetic field strength; however, as Schmahl *et al.* (1990) note, such a flat microwave spectrum cannot be explained with a simple homogeneous model, but requires instead an inhomogeneous source model with different turnover frequencies in different regions. During the rise phase of the flare the spectral index between 15.4 and 86.0 GHz was approximately -1.0; the major 86 GHz peak at 23:17:15 has a spectral index of -0.8 from 15.4 to 86 GHz. We note that the soft X-ray emitting material seen by GOES during this flare should have produced a peak flux of order 50 s.f.u. at radio wavelengths, with its time profile closely following the soft X-ray flux profile. The RSTN 15.4 GHz data (which shows about 20 s.f.u. near the GOES peak) could only be compatible with such a flux if the hot plasma was optically thick at 15.4 GHz, which would lead to a flux smaller than 50 s.f.u. The BIMA 86 GHz data can be compatible with such a flux provided that it was distributed on spatial scales much larger than 5″, as indeed we expect to be the case.

4.4. Flare 4

This was an optical class SF flare which began at about 19:22 UT on 1991 March 8; it reached a soft X-ray level of GOES class C7.5. The 86 GHz emission began at approximately 19:22:40 UT, and had a total duration of about 13 min. The accompanying microwave flare was observed at both Sagamore Hill and OVRO. The temporal profiles of this flare at 5, 8.8, 15.4, and 86 GHz (baseline 31), and the closure phase at 86 GHz, are shown in Figure 7. The optical flare location was 1″ from the BIMA pointing center, and 69″ from the OVRO pointing center.

The flare had a complex morphology at all frequencies. In the microwave range the initial sharp peak at 19:23:00 was the strongest; several more smaller peaks occur from 19:24 to 19:25, and then another broader peak occurs centered at 19:29 UT. The

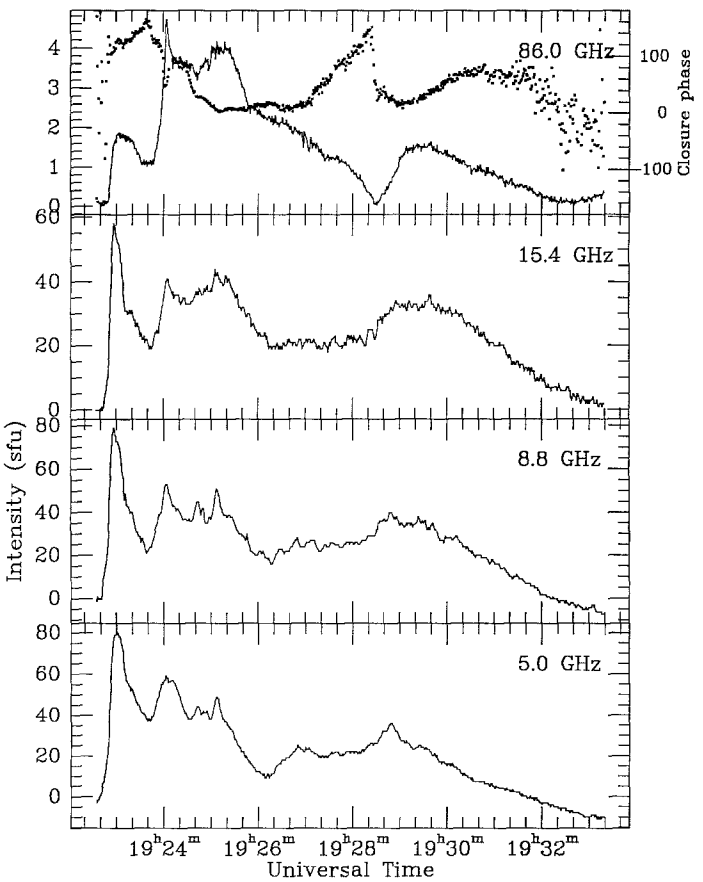

Fig. 7. Time profile of flare at 5.0, 8.8, 15.4, and 86.0 GHz (baseline 31); format as in Figure 1.

millimeter emission shows a sharp rise coincident with the first microwave peak, and other features corresponding to the different microwave peaks can also be seen. The three baselines at 86 GHz (fringe spacings of 4.5″, 9.8″, and 4.8″ on baselines 12, 23, and 31, respectively) all show the same features, but the relevant strengths of the different features differ on the different baselines. On baseline 12 the peak of 3 s.f.u. occurs in coincidence with the microwave peak at 19:25 UT; on baseline 23 the broad peak of 8 s.f.u. occurs in coincidence with the last microwave peak at 19:29 UT; while on baseline 31 the sharp peak of 5 s.f.u. occurs in coincidence with the microwave peak at 19:24 UT. This is consistent with the different peaks corresponding to physically different structures in the source, and further implies that again the overall source at 86 GHz was too large to be 'seen' with the available baselines. The 86 GHz closure phase data are consistent with this idea: the closure phase varied throughout the lifetime of the flare. The microwave peaks of the flare at 19:23 and 19:24–19:25 were resolved by OVRO at 15 GHz, implying a source size greater than 10″, whereas the peak at

19:29 was unresolved; all three microwave peaks, however, appear to originate from the same site.

The temporal profiles of the flare at 5.4 and 86.0 GHz (baseline 31) and in soft X-rays up to 19:27 UT are plotted together in Figure 8. Despite the fact that much of the 86 GHz flux is probably missing from the correlated amplitude shown, the temporal morphology of the flare at 86 GHz is remarkably similar to that in microwaves. Unlike the three previous flares, this time the soft X-ray emission begins before the impulsive phase in radio. There is a distinct time delay of ~ 5 s between the onset of the flare at 15.4 and 86 GHz, with the emission starting earlier at the lower frequency. One can show, as in the case of flare 1, that the time delay between the onset was not a consequence of the different effective detection thresholds at the two frequencies, but indicates a frequency dependence in the onset of the flare.

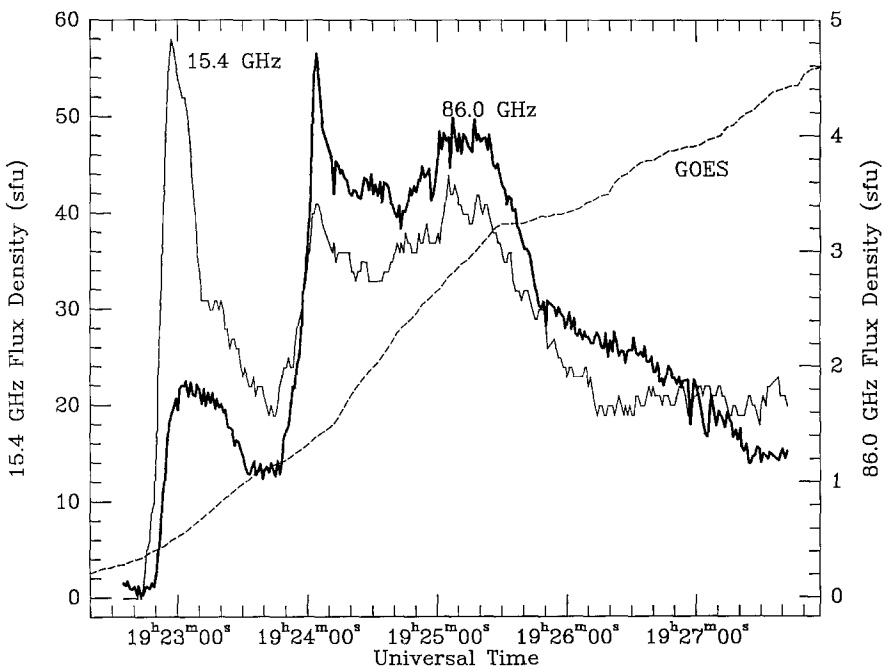

Fig. 8. Comparison of time profiles of flare 4 at 15.4 GHz (thin solid line), 86.0 GHz on baseline 31 (thick solid line), and in 3–25 keV soft X-rays (broken line).

During the initial microwave peak at 19:23 the radio emission has a spectral index of ~ 1.0 between 1.4 and 5.0 GHz, a flat spectrum between 5.0 and 8.8 GHz, and a spectral index of approximately 0.5 between 8.8 and 15.4 GHz. The turnover frequency is therefore between 5.0 and 15.4 GHz. During the rise phase of the flare the spectral index between 15.4 and 86.0 GHz was approximately -2.0. Thereafter, the microwave spectrum is essentially flat from 5 to 15 GHz, while the spectral index from 15.4 to 86 GHz has a minimum value of about -1.2. The soft X-ray emitting material can

contribute a flux of about 1 s.f.u. at 19:24, rising to a peak of about 2.5 s.f.u. at 19:30 UT.

4.5. FLARE 5

This is the weakest of all the flares reported in this paper. It occurred several minutes prior to a major flare (to be discussed next), and accordingly the data available in *Solar-Geophysical Data* do not give a clear picture of the optical properties. An importance 1B flare is listed as starting at 20:19 UT (1991 March 8), but at a position 62″ away from the center of the BIMA field-of-view. The emission at 86 GHz began at approximately 20:18:45 and had a total duration of only 30 s. The accompanying microwave mission was observed at Sagamore Hill, but not at OVRO because it occurred during a calibration scan. The temporal profiles of the flare at 5, 8.8, 15.4, and 86 GHz (baseline 12) are shown in Figure 9. The 86 GHz emission has a fast rise followed by a slower decay; the microwave emission appears to have the same morphology at 5.4 GHz, and is undetectable at lower frequencies. The microwave emission

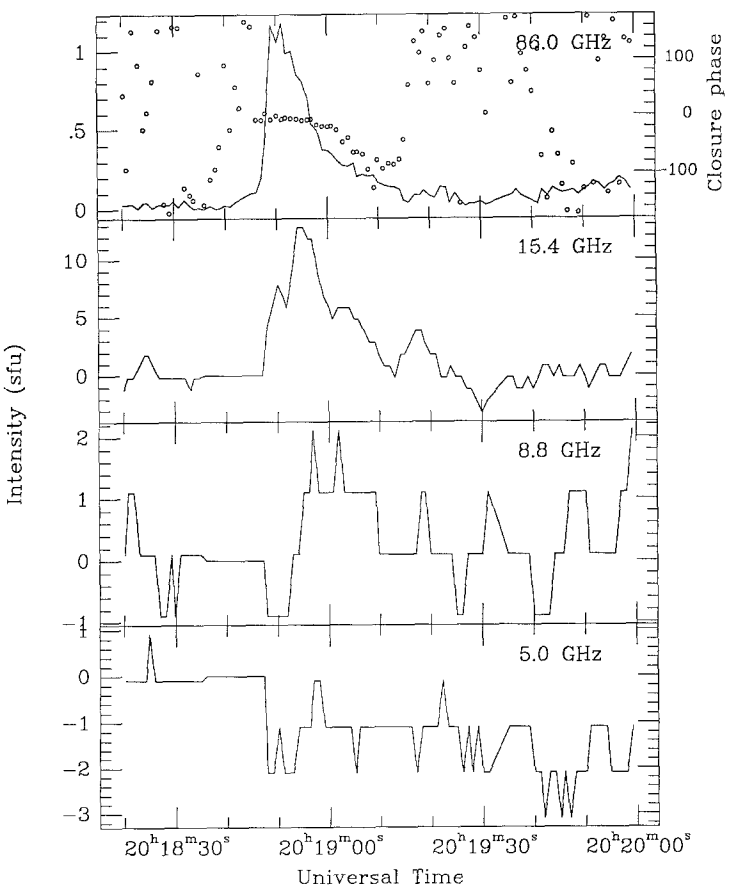

Fig. 9. Time profile of flare 5 at 5.0, 8.8, 15.4, and 86.0 GHz (baseline 23); format as in Figure 1.

is so weak that it seems unlikely that this event is associated with the 1B optical flare, and we believe that the optical event is not recorded.

The temporal profiles of the flare at 15.4 and 86.0 GHz, and the soft X-ray time profile, are plotted together in Figure 10. In this case there is no evidence for relative delays between the microwave and millimeter emission down to the 1 s time resolution of the RSTN data. The soft X-ray rise begins very close to the radio onset, and eventually reaches a level of C4.9.

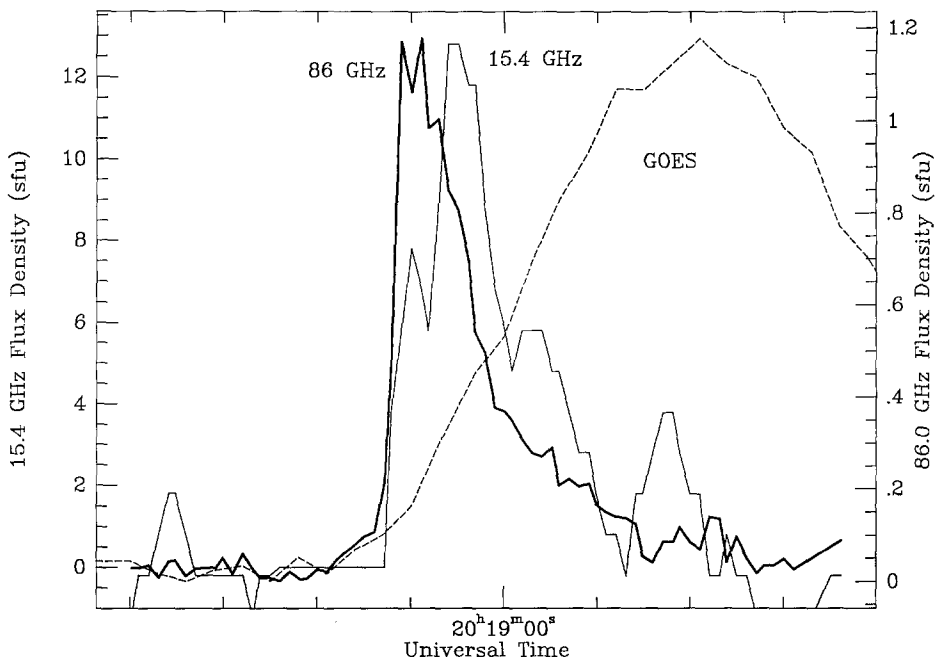

Fig. 10. Comparison of time profiles of flare 5 at 15.4 GHz (thin solid line), 86.0 GHz on baseline 12 (thick solid line), and in 3–25 keV soft X-rays (broken line).

The closure phase at 86.0 GHz remains constant throughout the lifetime of the burst (except perhaps very late in the decay phase), indicating that the source was simple on the scale of the available fringe spacings (5″, 9″, and 6″). The temporal morphology of the flare appears similar on all three baselines, but the flux on baseline 23 (peak of 1.3 s.f.u.) is slightly larger than on 12 (peak of 1.1 s.f.u.), while the flux on baseline 31 is much smaller (peak on 0.5 s.f.u. occurring 4 s after the peak on the other two baselines). Thus this burst was somewhat resolved on a 6″ baseline, implying a size of several arc sec.

The microwave burst has a spectral index $\gtrsim 3.0$ between 8.8 and 15.4 GHz. Given the low signal-to-noise of the microwave data, this may be consistent with an optically-thick homogeneous synchrotron source. The spectral index between 15.4 and 86 GHz

clearly varied as a function of time through the burst; using the peak fluxes at the two frequencies we obtain a value of -1.6 for the spectral index, but the true value was flatter early in the burst and steeper in the decay phase.

4.6. FLARE 6

This was another large flare (optical class 2B, soft X-ray class X1.7) which occurred at 20:20 UT on 1991 March 8. The 86 GHz emission began at approximately 20:25:30 on March 8, and had a total duration of over 10 min. The accompanying microwave flare was observed at both Sagamore Hill and OVRO. The temporal profile of this flare at 5, 8.8, 15.4, and 86 GHz (baseline 23) is shown in Figure 11; in Figure 12 we plot the time profiles at all 3 baselines at 86 GHz together with the 15.4 GHz profile. The optical flare location was 19″ from the BIMA pointing center, and 71″ from the OVRO pointing center.

In the microwave range this flare showed a relatively slow rise to a maximum at 20:27:20, followed by an initially sharp decay which then slowed. The 86 GHz peak

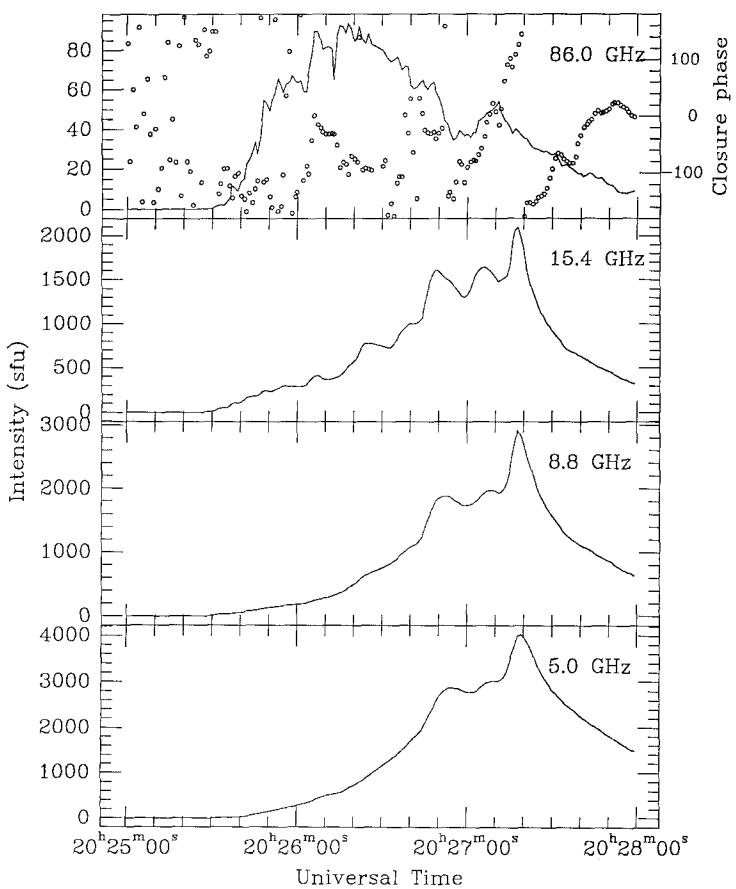

Fig. 11. Time profile of flare 6 at 5.0, 8.8, 15.4, and 86.0 GHz (baseline 23); format as in Figure 1.

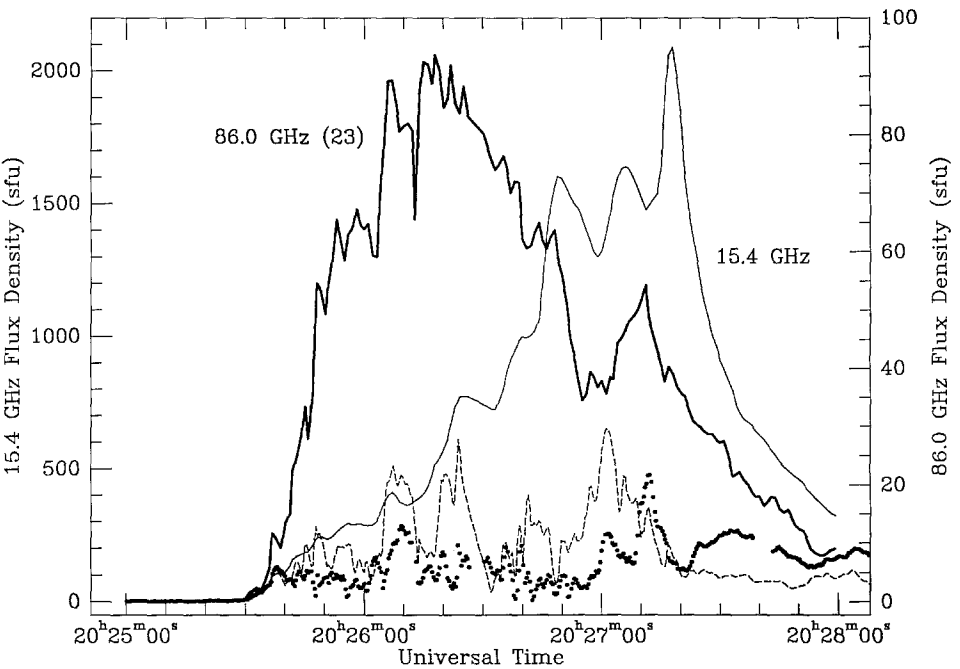

Fig. 12. Comparison of time profiles of flare 6 at 15.4 GHz (thin solid line), 86.0 GHz on baselines 23 (thick solid line), 12 (broken line) and 31 (filled circles).

on the shortest baseline (23) occurred 1 min earlier. We do not have the GOES data for this flare in digitized form; however, it may be found in *Solar-Geophysical Data*, and has an initial peak lasting perhaps 20 min, followed by a slowly decaying component.

In this event the different 86 GHz baselines (with fringe spacings of about 5″, 9″, and 6″, respectively) show little relationship to one another. The two longest baselines (12 and 31) show many short peaks, generally not coincident; the shortest baseline (23) shows a much smoother profile and much greater flux at all times (Figure 12). The closure phase at 86 GHz (Figure 11) varies on short times scales throughout the lifetime of the flare. The measured flux at 86 GHz starts to decay much earlier than that at microwaves, probably indicating that the source at 86 GHz rapidly became over-resolved. The microwave flare was well resolved at 15.4 GHz by OVRO, indicating that the source size was greater than 10″. All this evidence is consistent with a spatially very large microwave and millimeter source, unlike the other X-class flare (flare 3) discussed earlier.

The microwave flare had a spectral index of ~ 1.0 between 1.4 to 5.0 GHz, and a negative spectral index between 5.0 to 15.4 GHz. The turnover frequency therefore lies between 2.7 and 8.8 GHz. During the rise phase the spectral index between 15.4 and 86 GHz was at least -2.

5. Discussion

5.1. Properties of flare radio emission at 86 GHz

All these flares came from the same active region, and as a small sample they cannot be used to draw strong conclusions. However, some common properties stand out:

– in no case did the 86 GHz emission appear to start before the 15.4 GHz emission; however, there are two cases in which clear delays of the 86 GHz onset occurred, by about 5 s;

– in some cases the 86 GHz emission appears to be dominated by sources of dimension of order a few arc sec, even for very large flares; however, in most cases the source covers an extent larger than this. The interferometer is not sensitive to sources with uniform brightness distribution on scales larger than our largest fringe spacings ($\gtrsim 20''$);

– in no case is the 86 GHz emission dominated by the thermal bremsstrahlung contribution from the hot dense plasma seen in soft X-rays, at least on the spatial scale of up to $5''$ relevant to these observations;

– in those cases where not too much flux is missing at 86 GHz due to large source size, there is generally good agreement between the 15.4 and 86 GHz time profiles. In no cases, however, do they match in detail;

– the spectral index from 15.4 to 86 GHz is generally in the range -2 to -1 for these observations, and these numbers represent lower bounds because in most cases the total flux at 86 GHz was not measured.

We will use these properties to discuss the physics of flare emission at high frequencies.

5.2. Emission mechanism

The emission mechanism responsible for the impulsive phase of microwave flares is gyrosynchrotron emission (Dulk, 1985). For a homogeneous source, and electrons which have a power-law energy distribution, the radiation is expected to have a spectral index of ~ 2.9 in the optically thick regime, and in the optically thin regime a negative spectral index determined by the energy spectral index of the electrons (see below). For an inhomogeneous source, however, the optically thick spectral index is highly model-dependent. Of the six flares considered here only flares 1 and 5 have a low-frequency spectral index consistent with a homogeneous model. It is interesting that these were the two smallest bursts in this sample, and that both appeared to have very small sizes at 86 GHz. The optically thin spectral index is much less model-dependent, but because of the lack of sensitive observations at high frequencies it is not known in most cases.

The mechanisms which can produce detectable mm-wave emission from the Sun have been discussed by White *et al.* (1992) and White and Kundu (1992). Only two mechanisms are relevant at such high radio-frequencies, thermal bremsstrahlung and non-thermal gyrosynchrotron emission. Thermal gyrosynchrotron emission will not contribute at 86 GHz (Kundu *et al.*, 1990). The close temporal relationship between the

impulsive phase of the microwave and mm-wavelength emission suggests that the latter also is produced by gyrosynchrotron emission. Our comparison of GOES data and 86 GHz time profiles suggests than in most the cases the contribution of the soft X-ray emitting material to the 86 GHz flux during the early impulsive phase of the flare was weak, indicating that at this stage the emission of hot ($T \gtrsim 10^7$ K) thermal plasma is low, and therefore the contribution of this component to the mm-wave flux correspondingly weak. The soft X-ray flux peaks well after the impulsive phase, at which time the mm-wave flux also should be correspondingly high. During this time the soft X-ray source is generally large, however, and is over-resolved by the instrument. We cannot rule out the possibility that dense thermal material cooler than that seen by GOES is contributing to the 86 GHz emission in the impulsive phase; however, if so, it must be in a spatially separate location since the time taken for a dense two-temperature plasma to thermalize would be short. In a number of cases (flares 1 and 3) we can estimate brightness temperatures, which are lower limits to the actual mean energy of the radiating electrons. In both cases the brightness temperature is in excess of the temperature of the GOES material, and so cooler plasma cannot be responsible. Gary and Hurford (1989) obtained a similar result from microwave observations of a simple thermal burst: they found that the brightness temperature of the radio source exceeded that of the GOES material until late in the burst.

One great advantage of observing at 3.5 mm wavelength is that emission should almost always be optically thin; this is not the case even at 15.4 GHz, which can often easily be optically thick in high magnetic field regions during the impulsive phase of a flare. The negative spectral index of the radiation between microwave and mm frequencies found here confirms that the source is optically thin at mm-wavelengths. Although there are flares which appear to remain optically thick up to frequencies exceeding 90 GHz (Kaufmann *et al.*, 1985; White *et al.*, 1992), our study suggests that such flares occur only rarely.

5.3. Energy Spectrum of the Radiating Electrons

Generally we assume a power-law energy distribution for the electrons producing both the hard X-ray and radio emission in solar flares, that is, an electron number density of the form

$$n(E) = n_{E_0} \frac{\delta - 1}{E_0} \left(\frac{E}{E_0}\right)^{-\delta}, \tag{1}$$

where n_{E_0} is the total electron density at energies above a low-energy cutoff at E_0, and δ is the electron spectral index.

In the optically thin regime, the radio spectral index α is related to the electron spectral index δ by the expression (Dulk and Marsh, 1982)

$$\alpha = 1.22 - 0.90\delta \tag{2}$$

and this is not greatly altered by inhomogeneity in the source (e.g., see the models of

White, Kundu, and Jackson, 1989). In these observations we found that all the flares had radio spectral indices in the range -2.0 to -1.0 between 15.4 and 86.0 GHz; taking into account the missing flux at 86 GHz would raise these values. In two cases (flares 1 and 2) the turnover frequency may be above 15 GHz, but unless it is well above 15 GHz the resulting spectral index will not be greatly changed because of the large change in frequency from 15.4 to 86 GHz. Thus for these events energy spectral indices of at most 2.5 to 3.6 are implied.

The inferred range of electron spectral indices is somewhat lower than the range 3 to 5 commonly quoted in the microwave literature (e.g., Alissandrakis, 1986; Stahli, Gary, and Hurford, 1989). The latter were deduced from measurements at microwave frequencies, where the highest available frequency was often not much greater than the turnover frequency. Furthermore, the decrease in source size with increasing frequency may result in a negative spectral index in the optically thick regime, and this falling spectrum can be mistaken for optically thin emission. By contrast, for the flares presented here, the emission at mm wavelengths is undoubtedly optically thin and lies far above the turnover frequency.

The range of energy spectra deduced in these observations is also much lower than the range obtained from hard X-ray observations (typically $\delta = 4$ to 5), which are sensitive to the lower-energy range of the nonthermal distribution (Dennis, 1985). However, observations of large flares may be made to higher X-ray energies, and these often show a hardening of the energy spectrum above 300 keV (Dennis, 1988; Vestrand, 1988; McTiernan and Petrosian, 1991) which would be consistent with the flatter energy spectral indices found here.

Our selection procedure could lead to a bias for flares with relative strong mm-wave emission, and therefore those with relatively small electron spectral indices. The four flares discarded because of bad antenna pointing all had fluxes at 15.4 GHz which were about an order of magnitude greater than that at 86.0 GHz, and therefore had electron spectral indices similar to the six flares described above. The two flares discarded because of poor signal-to-noise ratios also had similar intensity ratios at 15.4 and 86.0 GHz. To see if any microwave flares without detectable mm-wave emission occurred during our observations, we searched the *Solar-Geophysical Data* records for microwave flares which were accompanied by Hα flares, and therefore those with known approximate positions. No new microwave flares were found with accompanying Hα flares which were in the field of view of the telescope. Thus the flares described appear to be free of any bias to flat energy spectra. It is, however, always possible that the particular active region observed produced flares with particularly hard energy spectra.

5.4. Total Energy of the Radio-Emitting Electrons

We can estimate the energy required to produce the electrons emitting at mm wavelengths from the flux with some assumptions. If V is the volume of the source, then the total energy of the radio-emitting electrons above some cutoff energy E_1 is, from (1),

$$E_T = \frac{\delta - 1}{\delta - 2} n_{E_0} V \left(\frac{E_1}{E_0}\right)^{-\delta+2} E_0 . \tag{3}$$

In order to use the standard approximate formulae for gyrosynchrotron emission of Dulk and Marsh (1982), we need to set $E_0 = 10$ keV, but for the low-energy cutoff to the energy distribution we will choose $E_1 = 25$ keV. The measured flux density is related to the emissivity by the expression (Dulk, 1985)

$$S = \eta \frac{V}{d^2} , \tag{4}$$

where η is the emissivity and d the distance to the Sun. For simplicity we will use the value $\delta = 3$ in place of the derived range of indices 2.5–3.6. Then the gyrosynchrotron emissivity at 86 GHz is (Dulk and Marsh, 1982)

$$\eta = 10^{-31.76} (\sin\theta)^{1.52} B^{2.5} n_{E_0} , \tag{5}$$

where θ is the angle between the magnetic field and the line of sight, and B is the magnetic field strength. Now we may use (4) to derive the total number of electrons above 10 keV from the measured flux

$$N_{E_0} = n_{E_0} V = 1.3 \times 10^{39} (\sin\theta)^{-1.52} B^{-2.5} S_{\text{s.f.u.}} . \tag{6}$$

The total energy above 5 keV is, by (3),

$$E_T = 1.8 \times 10^{31} (\sin\theta)^{-1.52} B^{-2.5} S_{\text{s.f.u.}} \text{ ergs} . \tag{7}$$

The total energy is thus a strong function of the magnetic field. In principle one can use the turnover frequency to estimate the magnetic field strength in the source (Dulk and Marsh, 1982), but in practise this is only true if the turnover frequency is determined by the same electrons which produce the millimeter emission, which is unlikely. Since millimeter emission should be strongest in the strongest magnetic fields one can generally assume $B = 300$–1000 G. For illustration we assume that $B = 500$ G and neglect the angle factor for an order-of-magnitude estimate: then the energy of the millimeter-emitting electrons at the peak of the X-class flares discussed here was about 4×10^{26} ergs. This is probably only a small fraction of the total energy in these large flares, and demonstrates that a small amount of energy in a flat-spectrum energy distribution can produce strong emission at high frequencies.

5.5. Delays and particle acceleration

Despite much theoretical effort, the processes responsible for the acceleration of particles during flares remain poorly understood. Nevertheless, strong and perhaps turbulent magnetic fields are believed to play a central role in this process. In the past, observations of the relative appearance time of particles with different energies have been used to place constraints on theoretical models. Our observations also are well suited for this purpose, since the impulsive microwave emission is probably produced by electrons with energies in the range 100 to 500 keV, whereas the corresponding mm-wave emission is produced by electrons with energies $\gtrsim 1$ MeV (White and Kundu, 1992).

As described above, two of the five flares studied (flares 1 and 4) showed a distinct time delay between the onset of the flare at microwave and mm wavelengths. The emission begins ~ 5 s earlier at microwaves than at 86 GHz. This time delay is reminiscent of the well studied time delay between the peaks of hard X-ray and microwave bursts. Lu and Petrosian (1990) have shown that for typical parameters delays as long as ~ 0.25 s could be caused by propagation effects (i.e., the time it takes for the high pitch-angle, high-energy electrons to mirror back upward can exceed the time taken by the low energy, low pitch-angle electrons to reach the footpoints), and because higher-energy electrons have longer lifetimes in a magnetic trap. Longer delays, however, require higher-energy electrons to be accelerated later than lower-energy ones. This conclusion is supported by observations of delays between the onset of hard X-ray flares at progressively higher energies (Bai and Dennis, 1985), and sudden increases in delay between the peaks of hard X-rays in adjacent energy channels (Bai and Ramaty, 1979). Furthermore, in a study of 93 hard X-ray bursts observed by the hard X-ray burst spectrometer (HXRBS) aboard the spacecraft SMM, Dulk, Kiplinger, and Winglee (1992) found that the majority of impulsive bursts displayed a time delay of a few seconds between the onset of hard X-rays at energies $\gtrsim 200$ keV compared to that at energies $\lesssim 100$ keV. Our observations of a time delay between the onset of the microwave and mm wavelength emission also appear to require that higher-energy electrons be accelerated later than lower-energy ones.

6. Conclusion

We have presented a study of the impulsive phase of solar flares at mm wavelengths. Such studies have been rare in the past and generally confined only to large and complex flares; with the greater sensitivity afforded by an interferometer we are able to study both large and small flares. For these events we found that in all cases the impulsive microwave flares which we could confidently identify as being in the field of view of the telescope were accompanied by mm-wave emission. Because gyrosynchrotron emission at mm wavelengths requires relativistic (i.e., $E \gtrsim 1$ MeV) electrons, our observations provide evidence that electrons are accelerated to very high energies during most if not all impulsive microwave flares.

The high-frequency radio spectral index has not been well-determined in the past. We found that for the flares observed here the spectral index of the radiation in the optically thin regime ranged from -1.0 to -2.0. For electrons with a power-law distribution in energy, the corresponding electron energy-spectral-index is in the range 2.5 to 3.6. In some cases the spectral indices were derived based on the assumption that the turnover frequency was not much above 15 GHz, and that the source was not too greatly over-resolved at 86 GHz; if the turnover frequency was higher the spectral index should be lower, and if the source was over-resolved the spectral index should be higher.

We find a delay in the onset of the flare at microwave and mm wavelengths with the emission beginning earlier at the lower frequency. This observation provides evidence

that, during an impulsive flare, higher-energy electrons are accelerated later than lower-energy electrons.

In a later paper we will use these results, together with conclusions from the comparison of millimeter and hard X-ray observations of another set of flares, to constrain models for particle acceleration in solar flares.

Acknowledgements

We are grateful to G. Deuel at NOAA/SEL for providing the RSTN network microwave data and to G. Labow at NASA/GSFC for providing the GOES data. Research at U. Md was supported by NSF grant ATM 90–19893 and AST 91–00306 and NASA grants NAG-5–1540, NAG-W-1541 and NAG-W-2172.

References

Akabane, K., Nakajima, K., Ohki, K., Moriyama, F., and Miyaji, T.: 1973, *Solar Phys.* **33**, 431.
Alissandrakis, C. E.: 1986, *Solar Phys.* **104**, 207.
Bai, T. and Dennis, B.: 1985, *Astrophys. J.* **292**, 699.
Bai, T. and Ramaty, R.: 1979, *Astrophys. J.* **227**, 1072.
Croom, D. L.: 1970, *Solar Phys.* **15**, 414.
Croom, D. L. and Powell, R. J.: 1969, *Nature* **221**, 945.
Dennis, B. R.: 1985, *Solar Phys.* **100**, 465.
Dennis, B. R.: 1988, *Solar Phys.* **118**, 49.
Dulk, G. A.: 1985, *Ann. Rev. Astron. Astrophys.* **23**, 169.
Dulk, G. A. and Marsh, K. A.: 1982, *Astrophys. J.* **259**, 350.
Dulk, G. A., Kiplinger, A. L., and Winglee, R. M.: 1992, *Astrophys. J.* **389**, 756.
Gary, D. E. and Hurford, G. J.: 1989, *Astrophys. J.* **339**, 1115.
Guidice, D. A. and Castelli, J. P.: 1975, *Solar Phys.* **44**, 155.
Hachenberg, O. and Wallis, G.: 1961, *Z. Astrophys.* **52**, 42.
Holt, S. S. and Ramaty, R.: 1969, *Solar Phys.* **8**, 119.
Hudson, H. S. and Ohki, K.: 1972, *Solar Phys.* **23**, 155.
Hurford, G. J., Read, R. B., and Zirin, H.: 1984, *Solar Phys.* **94**, 413.
Kaufmann, P., Correia, E., Costa, J. E. R., Vaz, A. M. Z., and Dennis, B. R.: 1985, *Nature* **313**, 380.
Kaufmann, P., Correia, E., Costa, J. E. R., and Vaz, A. M. Z.: 1986, *Astron. Astrophys.* **157**, 11.
Kawabata, K., Ogawa, H., Takakura, T., Tsuneta, S., Ohki, K., Yoshimori, M., Okudaira, K., Hirashima, Y., and Kondo, I.: 1982, in *HINOTORI Symposium on Solar Flares*, Institute of Space and Astronautical Sciences, Tokyo, p. 168.
Kundu, M. R., White, S. M., Gopalswamy, N., Bieging, J. H., and Hurford, G. J.: 1990, *Astrophys. J.* **358**, L69.
Lu, E. T. and Petrosian, V.: 1990, *Astrophys. J.* **354**, 735.
McTiernan, J. M. and Petrosian, V.: 1991, *Astrophys. J.* **379**, 381.
Ramaty, R.: 1969, *Astrophys. J.* **158**, 753.
Ramaty, R. and Petrosian, V.: 1972, *Astrophys. J.* **178**, 241.
Schmahl, E. J., Schmelz, J. T., Saba, J. L. R., Strong, K. T., and Kundu, M. R.: 1990, *Astrophys. J.* **358**, 654.
Shimabukuro, F. I.: 1970, *Solar Phys.* **15**, 424.
Shimabukuro, F. I.: 1972, *Solar Phys.* **23**, 169.
Stahli, M., Gary, D. E., and Hurford, G. J.: 1989, *Solar Phys.* **120**, 351.
Thomas, R. J., Starr, R., and Crannell, C.-J.: 1985, *Solar Phys.* **95**, 323.
Vestrand, W. T.: 1988, *Solar Phys.* **118**, 95.
White, S. M. and Kundu, M. R.: 1992, *Solar Phys.* (in press).
White, S. M., Kundu, M. R., and Jackson, P. D.: 1989, *Astron. Astrophys.* **225**, 112.
White, S. M., Kundu, M. R., Bastian, T. S., Gary, D. E., Hurford, G. J., Kucera, T., and Bieging, J. H.: 1992, *Astrophys. J.* **384**, 656.